Advanced Control Approach for Post-Fault Recovery in MTDC Networks

Sharma, Monika; Torres, José L.Rueda

DOI
10.1109/PowerTech59965.2025.11180617

Publication date
2025

Document Version
Final published version

Published in
2025 IEEE Kiel PowerTech, PowerTech 2025

Advanced Control Approach for Post-Fault Recovery in MTDC Networks

Monika Sharma, and José L. Rueda Torres
Department of Electrical Sustainable Energy, TU Delft, Delft, Netherlands
{ M.Sharma-3, J.L.RuedaTorres} @tudelft.nl

2025 IEEE Kiel PowerTech | 979-8-3315-4397-6/25/$31.00 ©2025 IEEE | DOI: 10.1109/PowerTech59965.2025.11180617

***Abstract*—The integration of renewable energy sources and offshore wind farms demands robust High-Voltage Direct Current (HVDC) networks. A key challenge is mitigating post-fault oscillations during converter deblocking, which arise from interactions between converter dynamics, HVDC cables, and system nonlinearities. These oscillations can destabilize the system, extend recovery times, and disrupt grid operations. This study investigates a four-terminal Multiterminal DC (MTDC) network using a real-time simulator. An enhanced DC voltage regulation strategy is proposed, integrating a washout filter and an anti-windup mechanism within a Proportional-Integral (PI) controller. Furthermore, a meticulous parametric sensitivity analysis is performed to optimize controller parameters, achieving significant reductions in oscillations using a real-time simulator to extract valuable insights into the damping method's effectiveness under various operating conditions.**

***Index Terms*—Active damping controller, Anti-windup mechanism, High Voltage Direct Current (HVDC) Network, Multi-Terminal DC (MTDC) Network, Wash-out-filter.**

I. Introduction

THE increasing deployment of offshore wind farms has heightened the demand for efficient power transmission systems to integrate large-scale renewable energy. Voltage-Sourced Converter (VSC)-based High-Voltage Direct Current (HVDC) networks are well-suited for this purpose, offering superior efficiency and controllability compared to traditional AC systems, which incur significant losses over long distances due to cable capacitance [1], [2]. VSC-HVDC networks enable advanced functionalities, such as Power Oscillation Damping (POD) and the development of Multi-Terminal HVDC (MTDC) networks for transnational renewable energy grids.

Modern VSC-HVDC systems commonly employ Modular Multi-level Converters (MMCs) due to their scalability and high performance. MMCs produce near-sinusoidal AC waveforms, minimizing filtering requirements at the Point of Common Coupling (PCC), and their modular design supports flexible expansion to meet rising energy demands [3], [4]. However, integrating HVDC networks into existing grids poses stability challenges, particularly during transient events like post-fault recovery. Poorly damped oscillations, arising from interactions between converter dynamics and the inductive-capacitive properties of long HVDC cables, can cause voltage instability, prolonged settling times, and system disruptions [5], [6].

Conventional damping methods, such as impedance-based and active damping, often fail to address the nonlinear dynamics of HVDC networks effectively. These approaches require additional hardware and face challenges in parameter tuning, limiting their efficacy [7], [8]. While advanced techniques like Model Predictive Control (MPC) reduce settling times by 13.6% [9], and virtual active damping maintains DC-link voltage stability [7], [10], most studies focus on point-to-point (P2P) HVDC configurations. Meshed HVDC networks, with their complex topologies and multi-modal interactions, remain underexplored, necessitating tailored control strategies [6], [11].

A significant gap in research exists regarding damping control in meshed HVDC networks compared to point-to-point (P2P) configurations. Most existing studies focus on P2P networks, neglecting the complex dynamics in meshed networks caused by their topologies and multi-modal interactions. This highlights the need for further investigation into control strategies tailored specifically to meshed HVDC networks [6], [11].

In this research, a novel damping control strategy is proposed to improve post-fault recovery in MTDC networks. The approach integrates DC voltage regulation with a washout filter and an anti-windup mechanism within a Proportional-Integral (PI) controller. The washout filter isolates oscillatory components, while the anti-windup mechanism prevents controller saturation during transients, improving stability and recovery.

The primary contributions of this study are summarized as follows:

- **Identification of optimal damping approaches:** Existing damping approaches are evaluated, and DC voltage regulation in MTDC networks is identified as essential for ensuring system stability [12] [13].
- **Development of an enhanced damping controller:** In damping control, a washout filter and anti-windup mechanism are integrated into the PI controller to improve oscillation control during post-fault recovery.

The paper is organized as follows: Section II discusses post-fault recovery challenges. Sections III and IV present the converter's mathematical model and the proposed damping control methodology, respectively. Section V analyzes the results, and Section VI concludes the study.

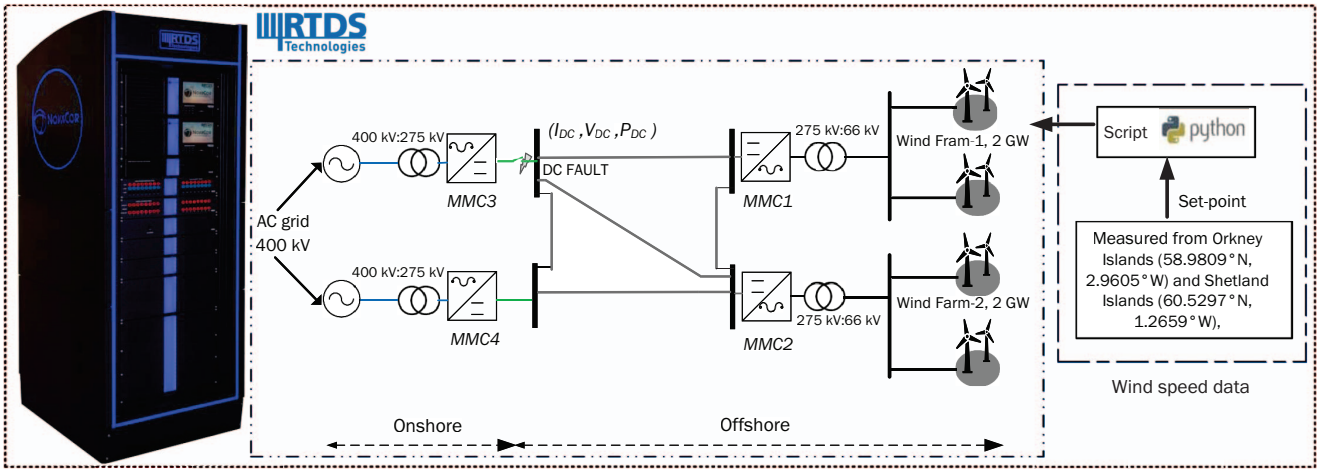

Fig. 1. A four-terminal ±525 kV half-bridge MMC-based MTDC network.

II. Challenges in Post-Fault Recovery

Post-fault recovery in High-Voltage Direct Current (HVDC) networks is critical for reliable operation following DC faults, often triggered by insulation breakdowns. These faults disrupt power flow, necessitating rapid recovery strategies to restore stability. Converters play a central role during Fault Ride-Through (FRT) conditions, which may require temporary blocking, significantly altering network dynamics [12].

Reactivating converters post-fault introduces challenges, including voltage and current oscillations and DC-side power fluctuations. Oscillation frequency depends on system parameters and chosen control strategies [12]. The primary objective of post-fault recovery is to restore DC voltage to pre-fault levels while minimizing oscillations, preventing over-currents, and avoiding over-voltages. Resonant frequencies, driven by the network's capacitive and inductive components (e.g., converters, cables, and inductors), can amplify oscillations, particularly during converter de-blocking at mismatched voltages.

Oscillations during converter de-blocking stem from complex interactions between converter dynamics and the HVDC network [12]. Their severity depends on the network's intrinsic damping and the controller's ability to suppress non-DC frequency components. Insufficient damping, influenced by DC Circuit Breakers (DCCBs), fault conditions, or network inductors, can exacerbate oscillations, risking over-voltages or over-currents on the DC side.

This study analyzes a four-terminal Modular Multi-level Converter (MMC)-based Multi-Terminal HVDC (MTDC) network with a ±525 kV DC voltage rating and a bipolar Dedicated Metallic Return (DMR) configuration, as shown in Fig. 1. The network, divided into onshore and offshore subsystems, employs half-bridge topology converters. Onshore converters (MMC3 and MMC4) connect to the Point of Common Coupling (PCC) via 12 km DC cables, with a DC hub incorporating a single switch for simplicity. The offshore subsystem includes MMC1 and MMC2, interfacing with aggregated wind farms modeled using an average-value approach. The subsea network includes five 300 km-long cable links, modeled using a frequency-dependent phase model. Each cable link comprises three conductors (positive, negative, and metallic return) to accommodate the DMR configuration. This setup ensures efficient and reliable operation of the MTDC network, integrating both onshore and offshore networks [14].

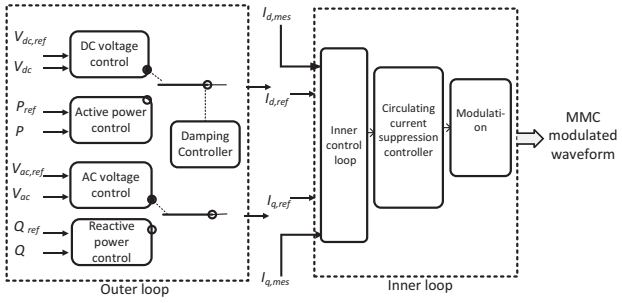

Fig. 2. Control loop design for MMC3 with damping integration.

Sub-Synchronous Oscillations (SSOs), occurring below the nominal system frequency during converter de-blocking, are a key focus. This study examines MMC3, which experiences SSOs following a short-circuit-induced blocking event near the onshore DC cable. SSOs cause power fluctuations and voltage deviations, threatening system stability and equipment integrity [15].

To address SSOs, a supplementary damping controller is integrated into the outer control loop of the converter, as depicted in Fig. 2. The controller takes the DC voltage error (V_{DC}^{err}), defined as the difference between the nominal and

measured DC voltages, as its input and generates a modulated signal (I_{DC}^{mod}) as its output, which is injected into the current control loop of the MMC-HVDC network. This modulated signal facilitates effective damping of SSOs by adjusting the DC current or voltage, thereby enhancing system stability during PF recovery.

This work highlights the need for advanced control strategies to stabilize MTDC networks during post-fault recovery. The proposed damping technique addresses SSOs, ensuring reliable operation of interconnected MTDC networks.

III. Mathematical DC-side Equivalent Circuit of the Converter

The interaction between a converter and an HVDC network during post-fault recovery can be effectively analyzed through its equivalent circuit on the DC side. The power balance factor, η, represents the ratio of AC power to DC power, defined as $\eta = \frac{P_{AC}}{P_{DC}}$, where $P_{AC} = \frac{3}{2} V_s I_s \cos(\phi)$ and $P_{DC} = V_{DC} I_{DC}$. The DC voltage of the converter, $V_{DC}(s)$, is expressed as a function of the DC current, $I_{DC}(s)$, η, and the zero-sequence component of the converter's internal voltage, $V_c^{*0}(s)$, as shown in Equation (1). Key parameters include V_s, I_s, and ϕ, which represent the peak values of the output AC voltage and current, and the phase shift between them, respectively.

$$\begin{aligned} V_{DC}(s) = \frac{1}{6}\left(\frac{3V_{DC}^{\sum}(0)}{sC_{sub}} - \frac{\eta}{s}\frac{3V_s I_s \cos(\phi)}{2V_{DC}C_{sub}} + \frac{NI_{DC}(s)}{sC_{sub}}\right) \\ + \frac{2}{3}L_{arm}\left(sI_{DC}(s) - i_{DC}(0)\right) \\ + \frac{2}{3}R_{arm}I_{DC}(s) - \frac{1}{3}\xi V_c^{*0}(s) \end{aligned} \tag{1}$$

In Equation (1), V_c^{*0}, represents the zero-sequence component of the internal voltage, which significantly impacts the DC voltage regulation of the converter. This voltage is managed by the Circulating Current Suppression Controller (CCSC), with various CCSC methods, including those based on D-Q coordinates, widely discussed in the literature [12], [16]–[18]. The D-Q-based method inherently determines the circulating current's DC component through the power exchange between the converter and the HVDC network. Consequently, in Equation (1), $V_c^{*0}(s)$ is set to zero for simplification.

At the de-blocking moment, immediately following fault clearance and transition to normal operation, it is assumed that $i_{DC}(0) = 0$ and no power exchange occurs ($\eta = 0$). Additionally, $V_{DC}^{\sum}(0)$ is approximated as twice the nominal DC voltage, $2V_{DC}^{n}$. These assumptions simplify Equation (1) into the reduced form shown in Equation (2).

To further clarify the converter's behavior during de-blocking, Fig. 3 presents a simplified circuit diagram of an MMC. The DC-side dynamics are influenced by key parameters, including the arm inductance (L_{arm}), arm resistance (R_{arm}), and the submodule capacitor (C_{sub}). These components seen collectively form the Thevenin equivalent circuit from the DC terminals, characterized by the impedance $Z_{c_i}^{DC}$.

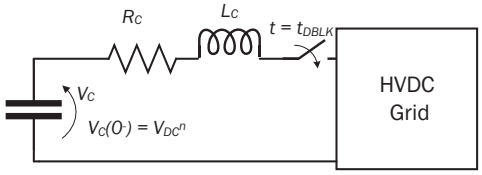

Fig. 3. Thevenin Equivalent Circuit of an MMC for DC Analysis.

$$\begin{aligned} V_{DC}(s) &= Z_{c_i}^{DC} I_{DC}(s) + \frac{V_{DC}^{n}}{s} \\ &\text{where} \\ Z_{c_i}^{DC} &= sL_{c_i} + R_{c_i} + \frac{1}{sC_{c_i}}, \\ L_{c_i} &= \frac{2}{3}L_{arm}, \quad R_{c_i} = \frac{2}{3}R_{arm}, \quad C_{c_i} = \frac{6C_{sub}}{N} \end{aligned} \tag{2}$$

Equation (2) represents the RLC equivalent circuit of the converter's DC side during de-blocking, where the pre-charged capacitor voltage V_{DC}^{n} creates an RLC configuration. The impedance $Z_{c_i}^{DC}$defines the DC current response, $I_{DC}(s)$.

Following de-blocking, the converter's recovery activates the RLC equivalent circuit. Oscillations may arise if the HVDC network voltage deviates from V_{DC}^{n} at the switching instant. While the RLC model accurately represents the system immediately after de-blocking, deviations from actual behavior may increase over time due to the influence of the power balance term η in Equation (1).

The activation of this equivalent circuit introduces transient electromagnetic oscillations, emphasizing the dynamic interactions between the converter and the network during post-fault recovery. Section IV delves into advanced damping methods to address these oscillations and improve system stability.

IV. Enhancement of the Damping Support Capability

This section introduces an advanced control methodology for DC-voltage regulation during the converter de-blocking phase, as depicted in Fig. 4. The proposed approach specifically targets the mitigation of oscillations triggered during de-blocking events. Following a fault clearance, the DC-side voltage often falls below a predefined threshold (V_{DC}^{min}), attributed to mismatches between the converter's output voltage and the grid-side DC voltage. These mismatches typically arise from limitations in conventional control schemes and voltage evaluation mechanisms.

The novel control strategy ensures precise alignment of the converter's DC-side voltage with the grid-side voltage by dynamically modulating the number of active submodules in the converter. By selectively reducing active submodules during the de-blocking phase, the proposed method effectively minimizes the voltage differential and mitigates the associated oscillations.

The control mechanism operates by deducting the control output from the internal voltage reference, which in turn decreases the number of active submodules. A dedicated signal, S_{DBLK}, activates the controller exclusively during de-blocking scenarios to enhance reliability and operational focus.

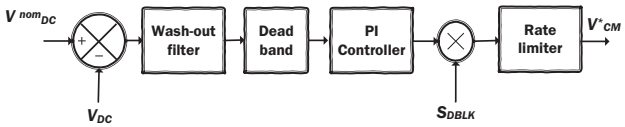

Fig. 4. Enhanced DC voltage regulation scheme for MTDC networks.

To further improve responsiveness, a washout filter is incorporated into the feedback loop of the enhanced DC voltage controller, as shown in Fig. 4. The washout filter, a high-pass filter, is designed to attenuate low-frequency components of voltage fluctuations, enabling the controller to rapidly address sudden changes in DC voltage while maintaining system stability. Its transfer function is given by:

$$G(s) = \frac{sT}{1+sT}, \tag{3}$$

where T is the time constant, tuned to optimize the filter's performance (see Section V for sensitivity analysis). The filter is implemented in the control loop to process the DC voltage error signal, ensuring that only transient high-frequency components are passed to the controller, thus preventing steady-state offsets from affecting the regulation process. This approach offers superior performance compared to traditional methods, such as low-pass filters, which may be less effective for managing significant low-frequency oscillations [12].

Additionally, a rate limiter governs the speed at which submodules are adjusted, ensuring smooth transitions during voltage regulation. By managing the rate of submodule insertion or removal, the limiter prevents abrupt voltage variations and promotes stable system operation.

The controller integrates the voltage error, defined as the difference between the nominal DC voltage and the grid voltage, to optimize performance during de-blocking. This integration enhances the system's dynamic response and ensures effective regulation of DC voltage deviations.

Under typical operating conditions, the controller remains inactive due to the proximity of the DC-side voltage to its nominal value, maintained by a dead-band block. However, if the DC-side voltage drops below V_{DC}^{min} during de-blocking, the controller output activates to adjust the number of inserted submodules, restoring alignment with the grid voltage [12].

Despite the benefits of integrating voltage error into the regulation process, challenges such as integrator windup can arise. Prolonged integration during saturated controller output may lead to undesirable effects, including oscillations, prolonged settling times, and reduced responsiveness during de-blocking [19].

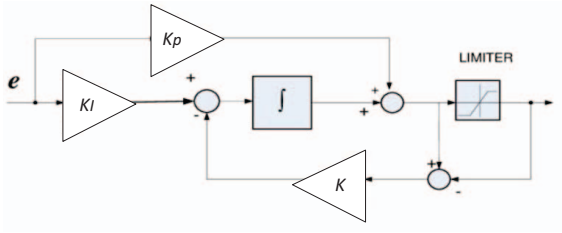

Fig. 5. Back-calculation-based anti-windup control for MTDC networks.

To address these challenges, an anti-windup mechanism, illustrated in Fig. 5, is integrated into the proposed DC voltage regulation scheme using the back-calculation method. While back-calculation is a well-established technique in control systems, its application in MTDC networks during converter de-blocking is tailored to mitigate integrator windup, which can otherwise lead to oscillations, prolonged settling times, and reduced responsiveness [19]. The anti-windup mechanism subtracts the surplus integrator output from its input, limiting the integrator's contribution during saturation. A proportional coefficient (k), set to $k = 1/k_p$, where k_p is the proportional gain of the PI controller, is used within the anti-windup loop to fine-tune performance based on system-specific requirements. The novelty of the proposed control strategy lies in the synergistic integration of the washout filter, rate limiter, and anti-windup mechanism, which collectively ensure robust DC voltage regulation and achieve significant performance improvements, including a 40.63% reduction in current overshoot and a 15.26% improvement in settling time (see Section V). This integrated approach enhances the stability of MTDC networks during post-fault recovery.

V. Simulation Results and Performance Analysis

The system model illustrated in Fig. 1 is simulated using the Real-Time Digital Simulator (RTDS), with the control loops detailed in Section II being employed. Electromagnetic transient (EMT) simulations are facilitated by RTDS integrated with RSCAD software, operated on specialized hardware such as PB5 cards or NovaCor units [20]. In this study, one NovaCor unit, equipped with seven cores, is utilized.

A four-terminal MTDC network, as depicted in Fig. 1, is employed for this study without DC circuit breakers. In Fig. 6, the initial voltages and currents on the DC side of the converter are presented. A severe DC fault, such as a short circuit near MMC3, is addressed by the immediate isolation of the fault through the opening of the DC-side switch, resulting in MMC3 being effectively blocked. After fault clearance, MMC3 is subsequently deblocked.

The impact of deblocking MMC3 on the voltages at all DC terminals (MMC1–MMC4) without an active damping controller is shown in Fig. 7. Significant voltage dips are observed near the DC-side converters during this process. Similarly, the current at the PCC near MMC3 during deblocking is depicted

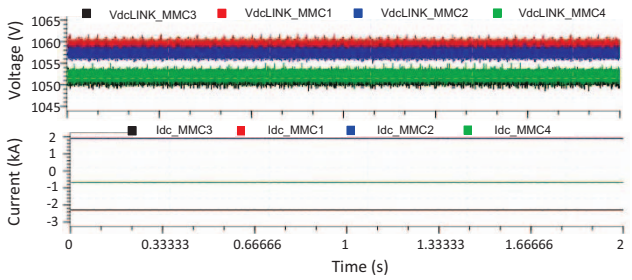

Fig. 6. Dynamic response of DC-side voltages and currents in the MTDC network.

in Fig. 8, where a peak overshoot of 1.1431 kA is recorded, along with a settling time of 0.15842 seconds.

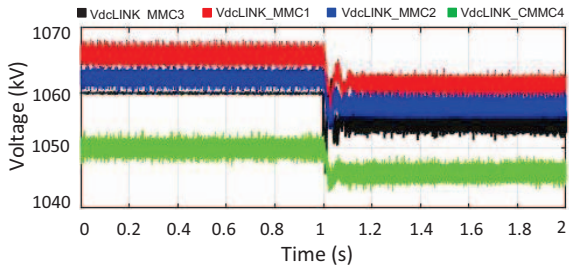

Fig. 7. Voltage response at converter terminals during deblocking.

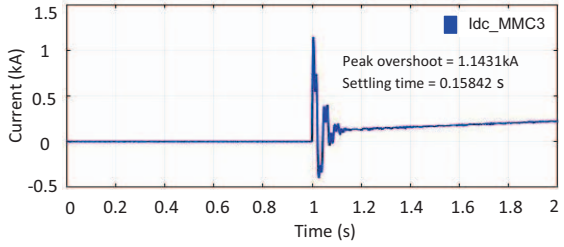

Fig. 8. Current Behavior at MMC3 Converter During De-blocking.

To enhance post-fault recovery, an advanced DC voltage regulation method is implemented as an active damping controller. A parametric sensitivity analysis is performed on the key parameters of the proposed controller, specifically the washout filter, to evaluate stability based on the relationship between Gain (G) and Time Constant (T). Experimental fine-tuning of G and T values is conducted. The results for various G and T combinations during the deblocking of MMC3 are summarized in Table I and Fig. 9. Optimal performance is achieved with a gain of 1 and a time constant of 0.09. Further variations in G and T have been found to result in increased peak overshoot and settling time. Similarly, sensitivity analysis is carried out for a PI controller with an anti-windup

TABLE I
SENSITIVITY ANALYSIS OF G AND T ON FILTER BEHAVIOR.

Gain (G)	Time Constant (T)	Peak Overshoot Value (kA)	Settling Time (s)
0.1	1	0.415061	0.142126
0.2	0.9	0.532060	0.168597
0.5	0.6	0.528170	0.156606
0.7	0.5	0.464277	0.157135
0.9	0.3	0.479046	0.157135
1	0.1	0.405200	00.149364
1	0.09	0.385615	0.149364
1.5	0.05	0.549708	0.159005
2	0.01	0.536784	0.133842

mechanism, yielding optimal values of 0.4 for the proportional gain (k_p), 0.7 for the integral time constant (T_i), and the anti-windup gain $k = 1/k_p = 2.5$. These parameters ensure optimal damping performance.

The comparative evaluation of the fine-tuned advanced controller ("Idc-PADC-ps") against the standard DC voltage active damping controller ("Idc-ADC"), the non-fine-tuned controller ("Idc-PADC"), and the baseline scenario without active damping control ("Idc-without-ADC") is presented in Table II and Fig. 10. The standard ADC employs default parameters as described in [12], without fine-tuning, to provide a baseline for evaluating the improvements achieved by the proposed controller's parametric optimization. During the deblocking process, the fine-tuned advanced controller ("Idc-PADC-ps") achieves a notable reduction in current overshoot by 40.63% and a decrease in settling time by 15.26% compared to the standard DC voltage controller, as illustrated in Fig. 10. This demonstrates the efficacy of the proposed controller in improving post-fault recovery.

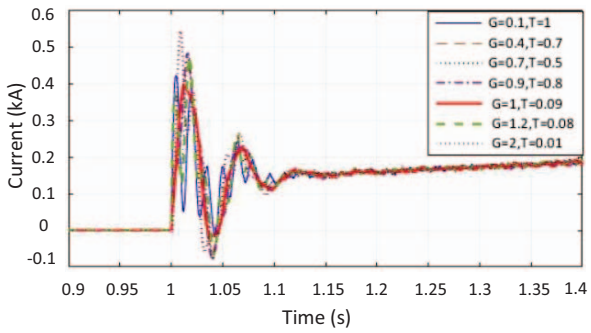

Fig. 9. Impact of Gain (G) and Time Constant (T) on System Performance

When no ADC is implemented, the current at the PCC near MMC3 during deblocking is represented by the orange dotted line in Fig. 10. This scenario results in a peak overshoot of 1.1431 kA and a settling time of 0.15842 seconds. Using the advanced fine-tuned controller, the overshoot is reduced

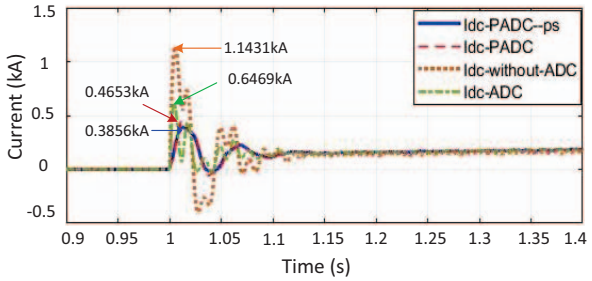

Fig. 10. Dyanmic performance evaluation of Enhanced ADC and comparison with existing controller.

TABLE II
PERFORMANCE EVALUATION OF ENHANCED CONTROLLER

Method	Paek-Overshoot value (kA)	Settling Time (s)
Fine-tuned Enhanced Controller	0.385615	0.149364
Standard ADC	0.649669	0.17627
Enhanced controller	0.465347	0.15038
No ADC	1.1431	0.15842

by 59. 28% and the settlement time is improved by 5.07% compared to the baseline case. Additionally, the enhanced controller with fine-tuned parameters outperforms the standard DC voltage regulator approach, achieving a 40.63% reduction in overshoot and a 15.26% improvement in settling time, thereby highlighting its effectiveness for post-fault recovery after severe DC faults [12].

VI. CONCLUSION

This research evaluates a four-terminal MTDC network, with a focus on post-fault recovery strategies for severe DC faults. The study underscores the significance of advanced damping methods, including washout filters and anti-windup mechanisms within PI controllers, in improving the resilience and stability of MTDC networks for practical applications. Enhanced damping controller demonstrates a 40.63% reduction in peak current overshoot and a 15.26% improvement in settling time when compared to the standard method. Furthermore, relative to the baseline scenario without active damping, the advanced controller achieves a 59.28% reduction in overshoot and a 5.07% improvement in settling time. These findings validate the efficacy of the enhanced controller in mitigating post-fault transients, enabling faster and more stable recovery of the MTDC network.

ACKNOWLEDGMENT

This work is supported by HVDC-WISE project which is European Union's Horizon Europe program under agreement 101075424. UK Research and Innovation (UKRI) funding for HVDC-WISE is provided under the UK government's Horizon Europe funding guarantee [grant numbers 10041877 and 10051113].

REFERENCES

[1] M. Saeedifard, M. Graovac, R. Dias, and R. Iravani, "Dc power systems: Challenges and opportunities," in *IEEE PES general meeting*, pp. 1–7. Minneapolis, MN, USA, 2010.

[2] S. Cole, K. Karoui, T. K. Vrana, O. B. Fosso, J. Curis, A. M. Denis, and C. C. Liu, "A european supergrid: Present state and future challenges," in *Proc. 17th Power Systems Computation Conference (PSCC)*. Stockholm, Sweden, 2011.

[3] H. Yang, Y. Dong, W. Li, and X. He, "Average-value model of modular multilevel converters considering capacitor voltage ripple," *IEEE Transactions on Power Delivery*, vol. 32, no. 2, pp. 723–732, 2016.

[4] N.-T. Trinh, M. Zeller, K. Wuerflinger, and I. Erlich, "Generic model of mmc-vsc-hvdc for interaction study with ac power system," *IEEE Transactions on Power Systems*, vol. 31, no. 1, pp. 27–34, 2015.

[5] J. H. Enslin and P. J. Heskes, "Harmonic interaction between a large number of distributed power inverters and the distribution network," *IEEE Transactions on Power Electronics*, vol. 19, no. 6, pp. 1586–1593, 2004.

[6] D. Van Hertem, M. Ghandhari, and M. Delimar, "Technical limitations towards a supergrid—a european prospective," in *2010 IEEE International Energy Conference*, pp. 302–309. Manama, Bahrain, 2010.

[7] C. Li, Y. Li, Y. Cao, H. Zhu, C. Rehtanz, and U. Häger, "Virtual synchronous generator control for damping dc-side resonance of vsc-mtdc system," *IEEE Journal of Emerging and Selected Topics in Power Electronics*, vol. 6, no. 3, pp. 1054–1064, 2018.

[8] G. Pinares and M. Bongiorno, "Modeling and analysis of vsc-based hvdc systems for dc network stability studies," *IEEE Transactions on Power Delivery*, vol. 31, no. 2, pp. 848–856, 2015.

[9] V. Virulkar and G. Gotmare, "Sub-synchronous resonance in series compensated wind farm: A review," *Renewable and Sustainable Energy Reviews*, vol. 55, pp. 1010–1029, 2016.

[10] N. Kumar, B. Singh, and B. K. Panigrahi, "Voltage sensorless based model predictive control with battery management system: for solar pv powered on-board ev charging," *IEEE Transactions on Transportation Electrification*, 2022.

[11] J. Deng, F. Cheng, L. Yao, J. Xu, B. Mao, X. Li, and R. Chen, "A review of system topologies, key operation and control technologies for offshore wind power transmission based on hvdc," *IET Generation, Transmission & Distribution*, vol. 17, no. 15, pp. 3345–3363, 2023.

[12] M. Abedrabbo, F. Z. Dejene, W. Leterme, and D. Van Hertem, "Hvdc grid post-dc fault recovery enhancement," *IEEE Transactions on Power Delivery*, vol. 36, no. 2, pp. 1137–1148, 2020.

[13] M. Sharma, P. Palensky, and J. L. R. Torres, "Emt simulation based parametric tuning of damping support in mmc-hvdc networks," in *2024 IEEE 33rd International Symposium on Industrial Electronics (ISIE)*, pp. 1–6. IEEE, 2024.

[14] A. Shetgaonkar, T. Karmokar, M. Popov, and A. Lekić, "Enhanced real-time multi-terminal hvdc power system benchmark models with performance evaluation strategies," in *CIGRE Sci Eng*, vol. 62, pp. 1–29, 2024.

[15] R. N. Damas, Y. Son, M. Yoon, S.-Y. Kim, and S. Choi, "Subsynchronous oscillation and advanced analysis: A review," *IEEE Access*, vol. 8, pp. 224 020–224 032, 2020.

[16] J. Pou, S. Ceballos, G. Konstantinou, V. G. Agelidis, R. Picas, and J. Zaragoza, "Circulating current injection methods based on instantaneous information for the modular multilevel converter," *IEEE Transactions on Industrial Electronics*, vol. 62, no. 2, pp. 777–788, 2014.

[17] J. Qin and M. Saeedifard, "Predictive control of a modular multilevel converter for a back-to-back hvdc system," *IEEE Transactions on Power delivery*, vol. 27, no. 3, pp. 1538–1547, 2012.

[18] X. She, A. Huang, X. Ni, and R. Burgos, "Ac circulating currents suppression in modular multilevel converter," in *IECON 2012-38th Annual Conference on IEEE Industrial Electronics Society*, pp. 191–196. Montreal, Canada, 2012.

[19] W. Liu, Y. Zheng, Q. Chen, and D. Geng, "An adaptive cgpc based anti-windup pi controller with stability constraints for the intermittent power penetrated system," *International Journal of Electrical Power & Energy Systems*, vol. 130, p. 106922, 2021.

[20] R. Technologies, *RTDS Technologies Website*, 2021. [Online]. Available: www.rtds.com